AIChE

Four Beds Pressure Swing Adsorption for Hydrogen Purification: Case of Humid Feed and Activated Carbon Beds

Ana M. Ribeiro, Carlos A. Grande, Filipe V. S. Lopes, José M. Loureiro, and Alírio E. Rodrigues
Laboratory of Separation and Reaction Engineering (LSRE), Associate Laboratory, Dept. of Chemical Engineering, Faculty of Engineering, University of Porto, Porto 4200-465, Portugal

DOI 10.1002/aic.11886
Published online July 22, 2009 in Wiley InterScience (www.interscience.wiley.com).

The novelty of this manuscript is the study of purification of hydrogen from a mixture of $H_2/CO_2/CH_4/CO/N_2$ saturated in water vapor. Simulations results of fixed bed behavior and of an eight steps PSA process are presented using an activated carbon as adsorbent. Several operating conditions were considered, namely different feed flow rates, humid/dry feed and adiabatic/nonadiabatic operation. Simulation with single column PSA showed that a 99.9979% purity hydrogen stream could be obtained with a recovery of 71.3% and a productivity of 63.9 mol_{H_2}/kg_{ads}/day. The simulation of a four columns PSA predicted a decrease in H_2 purity to 99.8193% for the same operating conditions, due to the impurities present in the recycled stream of the continuous multicolumn process. To increase the hydrogen purity above 99.99%, the feed time was decreased 25%. Thus, the multicolumn simulation predicted a hydrogen recovery, purity, and productivity, respectively, of 62.7%, 99.9992%, and 55.2 mol_{H_2}/kg_{ads}/day.
 AIChE J, 55: 2292–2302, 2009
Keywords: hydrogen purification, PSA, humid feed, mathematical modelling, dynamic simulation

Introduction

High purity hydrogen is used in many important industrial applications, namely hydrocracking, hydrogenation of fats and oils, methanol production, manufacture of silicon, etc. In addition, the recent environmental concerns have prompted developments in the fuel cell industry towards the replacement of fossil-fuels by hydrogen, with which water is released from the combustion instead of greenhouse gases. These developments led to an increasing demand for fuel grade hydrogen (above 99.99%) in the market with the resulting economic motivation for advanced research in the field of hydrogen production.

The production of hydrogen is normally done by catalytic reforming of natural gas combined with a water gas shift reaction step, from which a hydrogen stream containing several impurities, namely water vapor, carbon dioxide, methane, carbon monoxide, and nitrogen, is obtained. This stream has 70–72% of hydrogen, 15–20% of carbon dioxide, <4% of carbon monoxide, <8% of methane and is saturated with water.[1] In addition, if the methane employed as fuel contains nitrogen as contaminant, this gas will also be present in the off-gas of the reformer (<4%). These impurities must be removed in order to obtain the required high purity hydrogen. This separation is typically performed with a pressure swing adsorption (PSA) unit.[2,3]

Numerous experimental and theoretical studies of hydrogen purification by PSA can be found in the literature.[4–11] However, as mentioned earlier, water vapor is one of the impurities present in the feed stream of the hydrogen purification processes and must also be removed. This important aspect is in general neglected. Studies that consider humid feeds are normally restricted to air purification processes where carbon dioxide concentration is in the ppm level,[12–14]

Correspondence concerning this article should be addressed to A. E. Rodrigues at arodrig@fe.up.pt

that are not representative of hydrogen purification from exiting steam methane reforming (SMR) off-gases. One exception is the experimental work reported by Li et al.[15] on CO_2 capture from humid flue gas streams. Thus, fundamental studies dealing with the purification of hydrogen from a humid stream of $H_2/CO_2/CH_4/CO/N_2$ and the influence of water vapor on the process performance are lacking in the literature which is the main focus of this work.

The purpose of this work is to provide some insights into purification of hydrogen from a mixture of $H_2/CO_2/CH_4/CO/N_2$ saturated in water vapor. Simulations results both of fixed bed behavior and of a PSA process, considering an activated carbon bed, are presented. A PSA cycle scheme with eight steps, including two pressure equalization steps was used. This study supplies knowledge of the fundamental adsorption behavior of these mixtures, which are of interest in hydrogen storage and purification and consequently of potential hydrogen technology applications: hydrogenation of fats and oils, hydrocracking, methanol production, manufacture of silicon and, specially due to environmental concerns, the use of hydrogen for fuel cells.

Mathematical Model

To understand the dynamic behavior of a PSA process, a mathematical model coupling mass, momentum, and energy balances over a packed bed with the appropriate boundary conditions for each step of the PSA cycle is needed.

The mathematical model used in this study was obtained considering the following assumptions: (i) ideal gas behavior throughout the column; (ii) no mass, heat or velocity gradients in the radial direction; (iii) axial dispersed plug flow; (iv) external mass and heat transfer resistances expressed with the film model; (v) bidispersed adsorbent particle with macropore and micropore mass transfer resistances, both expressed with the linear driving force (LDF) model; (vi) no temperature gradients inside particles; (vii) the column wall interchanges energy with the gas phase inside the column and with the external environment: constant heat transfer coefficients and constant external environment were considered; (viii) constant porosity along the bed, (ix) the Ergun equation is valid locally, i.e., in the momentum balance, only the terms of pressure drop and velocity change are considered.

With these assumptions the following material balances over the bulk phase (1), the macropores (2) and the micropores (3) are obtained.

$$\frac{\partial}{\partial z}\left(\varepsilon D_{ax} C_{g,T}\frac{\partial y_i}{\partial z}\right) - \frac{\partial}{\partial z}(u_0 C_{g,i}) - \varepsilon\frac{\partial C_{g,i}}{\partial t} - \frac{(1-\varepsilon)a_p k_f}{1+Bi_i}\left(C_{g,i} - \overline{C_{p,i}}\right) = 0 \quad (1)$$

$$\frac{\partial \overline{C_{p,i}}}{\partial t} = \frac{\Omega_M D_{p,i} Bi_i}{R_p^2(1+Bi_i)}\left(C_{g,i} - \overline{C_{p,i}}\right) - \frac{\rho_p}{\varepsilon_p}\frac{\partial \overline{q_i}}{\partial t} \quad (2)$$

$$\frac{\partial \overline{q_i}}{\partial t} = \frac{\Omega_c D_{c,i}}{r_c^2}\left(q_i^* - \overline{q_i}\right) \quad (3)$$

In these equations z is the axial position, t is the time, ε is the bed porosity, u_0 is the superficial velocity, $C_{g,T}$ and $C_{g,i}$ are respectively the total and component i gas phase concentrations, y_i is the component i molar fraction, $\overline{C_{p,i}}$ is the average concentration of component i in the macropores, $\overline{q_i}$ is the particle averaged adsorbed concentration, q_i^* is the adsorbed concentration in equilibrium with $\overline{C_{p,i}}$, D_{ax} is the mass axial dispersion coefficient, k_f is the film mass transfer coefficient, $D_{p,i}$ is the macropore diffusivity of component i, $D_{c,i}$ is the micropore diffusivity of component i, Bi_i is the mass Biot number of component i $\left(Bi_i = \frac{a_p k_f R_p^2}{\varepsilon_p \Omega_M D_{p,i}}\right)$, R_p, a_p, ε_p, and ρ_p, are respectively the particle radius, specific area, porosity and density, Ω_M and Ω_c are the macropore and micropore LDF factors given by $[\Omega = (k_s+1)(k_s+3)]$ where k_s is the geometrical factor (0, slab; 1, cylinder; 2, sphere).

The energy balances take into consideration the three phases present: gas, solid, and column wall. The energy balance for the gas phase is given by:

$$\frac{\partial}{\partial z}\left(\lambda\frac{\partial T_g}{\partial z}\right) - u_0 C_{g,T} C_p \frac{\partial T_g}{\partial z} + \varepsilon R_g T_g \frac{\partial C_{g,T}}{\partial t} - (1-\varepsilon)a_p h_f (T_g - T_p) - \frac{4h_w}{d_{wi}}(T_g - T_w) - \varepsilon C_{g,T} C_V \frac{\partial T_g}{\partial t} = 0 \quad (4)$$

where T_g, T_p, and T_w are respectively gas phase, solid phase and wall temperatures, C_v is the gas mixture molar specific heat at constant volume, C_p is the gas mixture molar specific heat at constant pressure, λ is the heat axial dispersion coefficient, h_f is the film heat transfer coefficient between the gas and particle, h_w is the film heat transfer coefficient between the gas and wall, R_g is the ideal gas constant and d_{wi} is the internal bed diameter.

The solid phase energy balance is expressed by:

$$(1-\varepsilon)\left[\varepsilon_p \sum_{i=1}^{n}\overline{C_{p,i}}C_{v,i} + \rho_p \sum_{i=1}^{n}\overline{q_i}C_{v,ads,i} + \rho_p \hat{C}_{ps}\right]\frac{\partial T_p}{\partial t} = (1-\varepsilon)\varepsilon_p R_g T_p \frac{\partial \overline{C_{p,T}}}{\partial t} + \rho_b \sum_{i=1}^{n}(-\Delta H_{ads})_i \frac{\partial \overline{q_i}}{\partial t} + (1-\varepsilon)a_p h_f (T_g - T_p) \quad (5)$$

where ρ_b is the bed density, $\hat{C}_{ps}$ is the particle specific heat at constant pressure (per mass unit), $C_{v,ads,i}$ is the molar specific heat of component i in the adsorbed phase at constant volume and $(\Delta H_{ads})_i$ is the heat of adsorption of component i.

The energy balance around the column wall is represented by:

$$\rho_w \hat{C}_{p,w}\frac{\partial T_w}{\partial t} = \alpha_w h_w (T_g - T_w) - \alpha_{wf} U (T_w - T_\infty) \quad (6)$$

where T_∞ is the ambient temperature, $\hat{C}_{pw}$ is the wall specific heat at constant pressure (per mass unit), ρ_w is the wall density, α_w is the ratio of the internal surface area to the volume of the column wall and $\alpha_{w\ell}$ is the ratio of the log mean surface to the volume of column wall.

As mentioned earlier, Ergun equation (7) is considered valid locally, i.e., in each z position the following relation holds:

Table 1. Boundary Conditions Associated with the Steps Commonly Used in PSA Operation

Co-current pressurization with feed	
Inlet, $z = 0$	$z = L$
$u_{0\text{inlet}} C_{\text{inlet},i} = u_0\, C_{\text{g},i} - \varepsilon D_{\text{ax}} C_{\text{g,T}} \dfrac{\partial y_i}{\partial z}$	$\dfrac{\partial C_{\text{g},i}}{\partial z} = 0$
$P = P_{\text{inlet}}$	$u_0 = 0$
$u_{0\text{inlet}} C_{\text{inlet},T} C_p T_{\text{inlet}} = u_0\, C_{\text{g,T}} C_{\text{p}} T_{\text{g}} - \lambda \dfrac{\partial T_{\text{g}}}{\partial z}$	$\dfrac{\partial T_{\text{g}}}{\partial z} = 0$
Counter-current pressurization with the less adsorbed compound	
$z = 0$	Inlet, $z = L$
$\dfrac{\partial C_{\text{g},i}}{\partial z} = 0$	$u_{0\text{inlet}} C_{\text{inlet},i} = u_0\, C_{\text{g},i} - \varepsilon D_{\text{ax}} C_{\text{g,T}} \dfrac{\partial y_i}{\partial z}$
$u_0 = 0$	$P = P_{\text{exit}}$
$\dfrac{\partial T_{\text{g}}}{\partial z} = 0$	$u_{0\text{inlet}} C_{\text{inlet,T}} C_{\text{p}} T_{\text{inlet}} = u_0\, C_{\text{g,T}} C_{\text{p}} T_{\text{g}} - \lambda \dfrac{\partial T_{\text{g}}}{\partial z}$
Feed	
Inlet, $z = 0$	Outlet, $z = L$
$u_{0\text{inlet}} C_{\text{inlet},i} = u_0\, C_{\text{g},i} - \varepsilon D_{\text{ax}} C_{\text{g,T}} \dfrac{\partial y_i}{\partial z}$	$\dfrac{\partial C_{\text{g},i}}{\partial z} = 0$
$u_{0\text{inlet}} C_{\text{inlet,T}} = u_0 C_{\text{g,T}}$	$P = P_{\text{exit}}$
$u_{0\text{inlet}} C_{\text{inlet,T}} C_{\text{p}} T_{\text{inlet}} = u_0\, C_{\text{g,T}} C_{\text{p}} T_{\text{g}} - \lambda \dfrac{\partial T_{\text{g}}}{\partial z}$	$\dfrac{\partial T_{\text{g}}}{\partial z} = 0$
Counter-current blowdown	
Outlet, $z = 0$	$z = L$
$\dfrac{\partial C_{\text{g},i}}{\partial z} = 0$	$\dfrac{\partial C_{\text{g},i}}{\partial z} = 0$
$P = P_{\text{exit}}$	$u_0 = 0$
$\dfrac{\partial T_{\text{g}}}{\partial z} = 0$	$\dfrac{\partial T_{\text{g}}}{\partial z} = 0$
Counter-current purge with the less adsorbed compound	
Outlet, $z = 0$	Inlet, $z = L$
$\dfrac{\partial C_{\text{g},i}}{\partial z} = 0$	$u_{0\text{inlet}} C_{\text{inlet},i} = u_0\, C_{\text{g},i} - \varepsilon D_{\text{ax}} C_{\text{g,T}} \dfrac{\partial y_i}{\partial z}$
$P = P_{\text{exit}}$	$u_{0\text{inlet}} C_{\text{inlet,T}} = u_0 C_{\text{g,T}}$
$\dfrac{\partial T_{\text{g}}}{\partial z} = 0$	$u_{0\text{inlet}} C_{\text{inlet,T}} C_{\text{p}} T_{\text{inlet}} = u_0\, C_{\text{g,T}} C_{\text{p}} T_{\text{g}} - \lambda \dfrac{\partial T_{\text{g}}}{\partial z}$
Co-current rinse with the most adsorbed compound	
Inlet, $z = 0$	Outlet, $z = L$
$u_{0\text{inlet}} C_{\text{inlet},i} = u_0\, C_{\text{g},i} - \varepsilon D_{\text{ax}} C_{\text{g,T}} \dfrac{\partial y_i}{\partial z}$	$\dfrac{\partial C_{\text{g},i}}{\partial z} = 0$
$u_{0\text{inlet}} C_{\text{inlet,T}} = u_0\, C_{\text{g,T}}$	$P = P_{\text{exit}}$
$u_{0\text{inlet}} C_{\text{inlet,T}} C_{\text{p}} T_{\text{inlet}} = u_0\, C_{\text{g,T}} C_{\text{p}} T_{\text{g}} - \lambda \dfrac{\partial T_{\text{g}}}{\partial z}$	$\dfrac{\partial T_{\text{g}}}{\partial z} = 0$
Pressure equalization–depressurization	
$z = 0$	*Outlet*, $z = L$
$\dfrac{\partial C_{\text{g},i}}{\partial z} = 0$	$\dfrac{\partial C_{\text{g},i}}{\partial z} = 0$
$u_0 = 0$	$P = P_{\text{exit}}$
$\dfrac{\partial T_{\text{g}}}{\partial z} = 0$	$\dfrac{\partial T_{\text{g}}}{\partial z} = 0$

(*Continued*)

Table 1. (Continued)

	Pressure equalization–pressurization	
$z = 0$		Inlet, $z = L$
$\frac{\partial C_{g,i}}{\partial z} = 0$		$u_{0inlet} C_{inlet,i} = u_0 C_{g,i} - \varepsilon D_{ax} C_{g,T} \frac{\partial y_i}{\partial z}$
$u_0 = 0$		$u_{0inlet} C_{inlet,T} = u_0 C_{g,T}$
$\frac{\partial T_g}{\partial z} = 0$		$u_{0inlet} C_{inlet,T} C_p T_{inlet} = u_0 C_{g,T} C_p T_g - \lambda \frac{\partial T_g}{\partial z}$

$$-\frac{\partial P}{\partial z} = \frac{150\mu(1-\varepsilon)^2}{\varepsilon^3 d_p^2} u_0 + \frac{1.75(1-\varepsilon)\rho}{\varepsilon^3 d_p} |u_0| u_0 \qquad (7)$$

In this equation ρ and μ are respectively the bulk gas mixture density and viscosity.

A PSA cycle is a sequence of elementary steps. To properly simulate a PSA process, the conservation equations presented earlier should be coupled with the appropriate boundary conditions for each step. The boundary conditions associated with the most common steps found in a PSA process (pressurization, feed, blowdown, purge, rinse, and pressure equalization) are given in Table 1.

The adsorbent considered was an activated carbon. In particular, an activated carbon prepared by modification of a commercial sample of activated carbon extrudates by physical activation with carbon dioxide. This adsorbent was prepared within the framework of the European research project Hy2Seps (hybrid hydrogen-carbon dioxide separation systems)[16] with the purpose of enhancing its adsorption capacity for the impurities present in the hydrogen purification processes and was denominated AC5-KS[17] The adsorption isotherms of H_2, CO_2, CH_4, CO, N_2, and H_2O on the activated carbon were previously determined by a gravimetric method and fitted[17] with the Virial Isotherm[18,19] truncated after the second Virial term (8).

$$P = \frac{q}{K_H} \exp\left(\frac{2}{S} A q + \frac{3}{2S^2} B q^2\right) \qquad (8)$$

In this equation, S is the adsorbent specific surface area, A and B are the virial coefficients, and K_H is the Henry constant. The Henry constant is related to the temperature through the Van't Hoff equation:

$$K_H = K_\infty \exp\left(\frac{-\Delta H}{R_g T}\right) \qquad (9)$$

where K_∞ is the adsorption constant at infinite temperature and $(-\Delta H)$ is the heat of adsorption at zero coverage. The temperature dependency of the Virial coefficients are given through the following equations:

$$A = \sum_{m=0}^{\infty} \frac{A_m}{T^m}, B = \sum_{m=0}^{\infty} \frac{B_m}{T^m} \qquad (10)$$

The fitting parameters obtained are presented in Table 2.[17]

The Virial isotherm was chosen due to its flexibility to fit data with different degrees of steepness, as is the case encountered in this study where the isotherms of H_2, CO_2, CH_4, CO, and N_2 are of Type I and the isotherm of H_2O is of Type V. Another advantage of the Virial isotherm is that it allows the prediction of multicomponent adsorption directly from the monocomponent data through analytical expressions. The multicomponent adsorption equilibrium was then predicted using the extension of the Virial isotherm to multicomponent systems (11) proposed by Taqvi and LeVan[20]:

$$P_i = \frac{q_i}{K_{Hi}} \exp\left(\frac{2}{S} \sum_{j=1}^{N} A_{ij} q_j + \frac{3}{2S^2} \sum_{j=1}^{N} \sum_{k=1}^{N} B_{ijk} q_j q_k\right) \qquad (11)$$

Taqvi and LeVan[20] studied and compared quantitatively two predictive approaches (Method 1 and Method 2), the correlative approach and the ideal adsorbed solution theory (IAST). Since the two predictive methods give similar results, the second method was chosen and thus the mixing Virial coefficients were calculated by Eqs. 12 and 13

$$A_{ij} = \frac{(A_i + A_j)}{2} \qquad (12)$$

$$B_{ijk} = \frac{(B_i + B_j + B_k)}{3} \qquad (13)$$

Table 2. Virial Adsorption Isotherm Fitting Parameters on Modified Activated Carbon AC5-KS

Compound	K_∞ [mol/(kg bar)]	$-\Delta H$ (J/mol)	$A_0 \times 10^{-5}$ (m^2/mol)	$A_1 \times 10^{-6}$ (m^2K/mol)	$B_0 \times 10^{-11}$ (m^4/mol^2)	$B_1 \times 10^{-11}$ (m^4K/mol^2)
CO_2	8.06×10^{-5}	28017	0.081	45.31	0.365	92.247
H_2	2.16×10^{-3}	7256	−7.547	287.0	3.264	−899.4
CH_4	2.18×10^{-4}	23002	5.140	−84.54	−0.100	4.89×10^{-6}
CO	7.29×10^{-5}	23225	−2.148	140.5	−0.100	-3.23×10^{-4}
N_2	2.94×10^{-4}	18273	2.469	−11.62	−0.100	-3.30×10^{-4}
H_2O	1.93×10^{-6}	45928	−0.968	4.906	0.025	0.960

$S = 971$ m^2/g.

Table 3. Operating Conditions Used in the Breakthrough Curve Simulations

Column length (m)	0.445
Column diameter (m)	0.0721
Temperature (K)	303
Pressure (bar)	7
Adsorbent	Activated carbon AC5-KS
Mass of adsorbent (kg)	0.855
Bed porosity	0.40
Feed molar fraction (dry basis, %)	73.3 H_2; 16.6 CO_2; 3.5 CH_4; 2.9 CO; 3.7 N_2
Feed flow rate (SLPM, space time, s)	1.88 (160); 7.54 (40) and 15.08 (20)

The extension of the Virial model for a multicomponent mixture of the five gases plus water is purely exploratory. This is the first step to evaluate the performance of the PSA unit. It also provides the operating conditions where it is necessary to determine adsorption equilibrium data of the whole system (P, T, and molar fractions) reducing significantly the volume of experiments.

Results and Discussion

Breakthrough curve simulations

The aforementioned model was first applied for the simulation of fixed-bed behavior. The feed stream considered in the simulations was a mixture of H_2, CO_2, CH_4, CO, and N_2 saturated in water vapor at 303 K and at a total pressure of 7 bar. Several feed flow rates were assumed. The information on the different operating conditions employed, including the bed dimensions, is summarized in Table 3. As can be seen from the model equations, the values of some transport parameters are needed for the simulations. These were calculated employing frequently used correlations and the values obtained are presented in Table 4. Namely, the axial mass and heat dispersion coefficients, as well as, the mass transfer and heat convective coefficient were estimated using the Wakao and Funazkri correlations.[3,21,22] The internal convective heat transfer coefficient between gas and the column wall was calculated with the Wasch and Froment correlation.[23] Both adiabatic and nonadiabatic operations were considered. The macropore diffusivity took into account only the molecular diffusivities which were calculated with the Chapman-Enskog equation.[24] General properties of the gases, like density, viscosity, and molar specific heat were obtained according to Bird et al.[24] Breakthrough experiments were used to determine the transport kinetics of pure gases through moment analysis of the pulse response, i.e., derivative of the diluted breakthrough curve.[17] The micropore diffusivities were calculated based on the experimental values of the moments together with estimated values of axial dispersion coefficients, molecular, and macropore diffusivities.[25] The specific heat and the viscosity of the gas were estimated at the inlet conditions and taken as constant

Table 4. Transport Parameters Values Used in the Breakthrough Curve Simulations

D_p (m^2/s)*	CO_2: 3.38×10^{-6}
	H_2: 5.01×10^{-6}
	CH_4: 3.04×10^{-6}
	CO: 3.00×10^{-6}
	N_2: 3.00×10^{-6}
	H_2O: 2.95×10^{-6}
D_c/r_c^2 (s^{-1})*	CO_2: 3.31×10^{-2}
	H_2: 1.58
	CH_4: 1.46×10^{-2}
	CO: 6.77×10^{-2}
	N_2: 1.34×10^{-2}
	H_2O: 2.00×10^{-3}
k_f (m/s)	5.82×10^{-3}
h_f (W/m^2K)	98
h_w (W/m^2K)	62
U (W/m^2K)	15 or 0 (nonadiabatic or adiabatic)

*Values at inlet conditions.

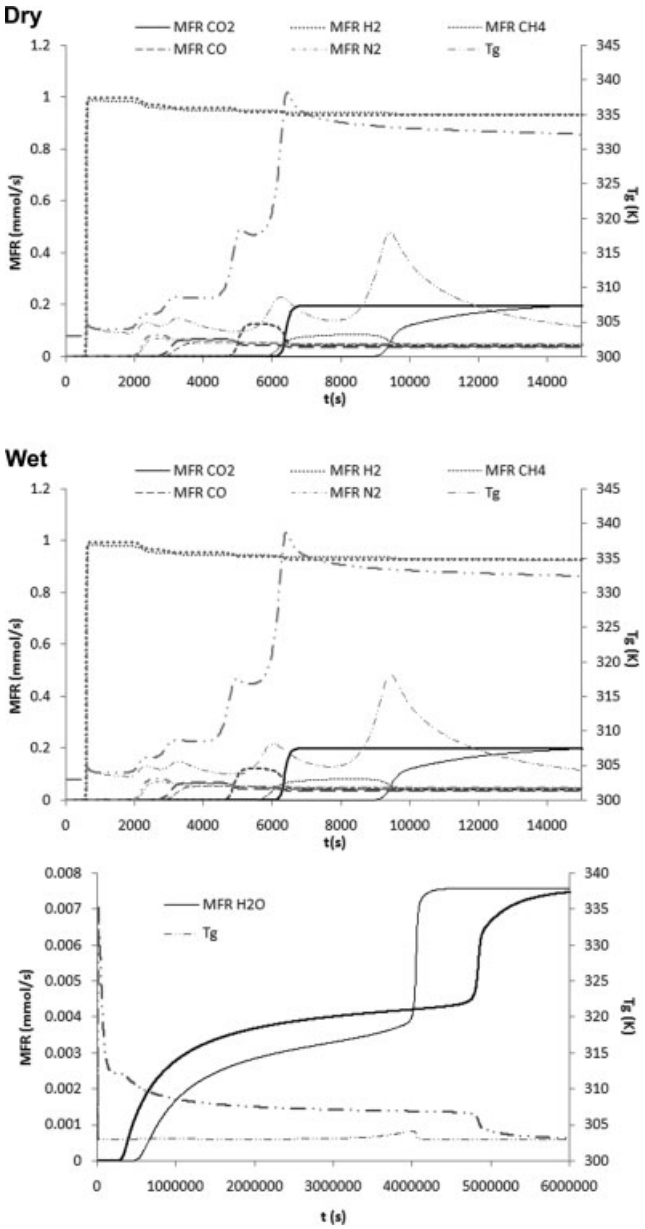

Figure 1. Molar flow rate and temperature histories at the column outlet obtained from the simulations with τ = 160 s.

The feed stream was either dry or saturated with water (wet) and both adiabatic (thick lines) and nonadiabatic (thin lines) conditions were considered.

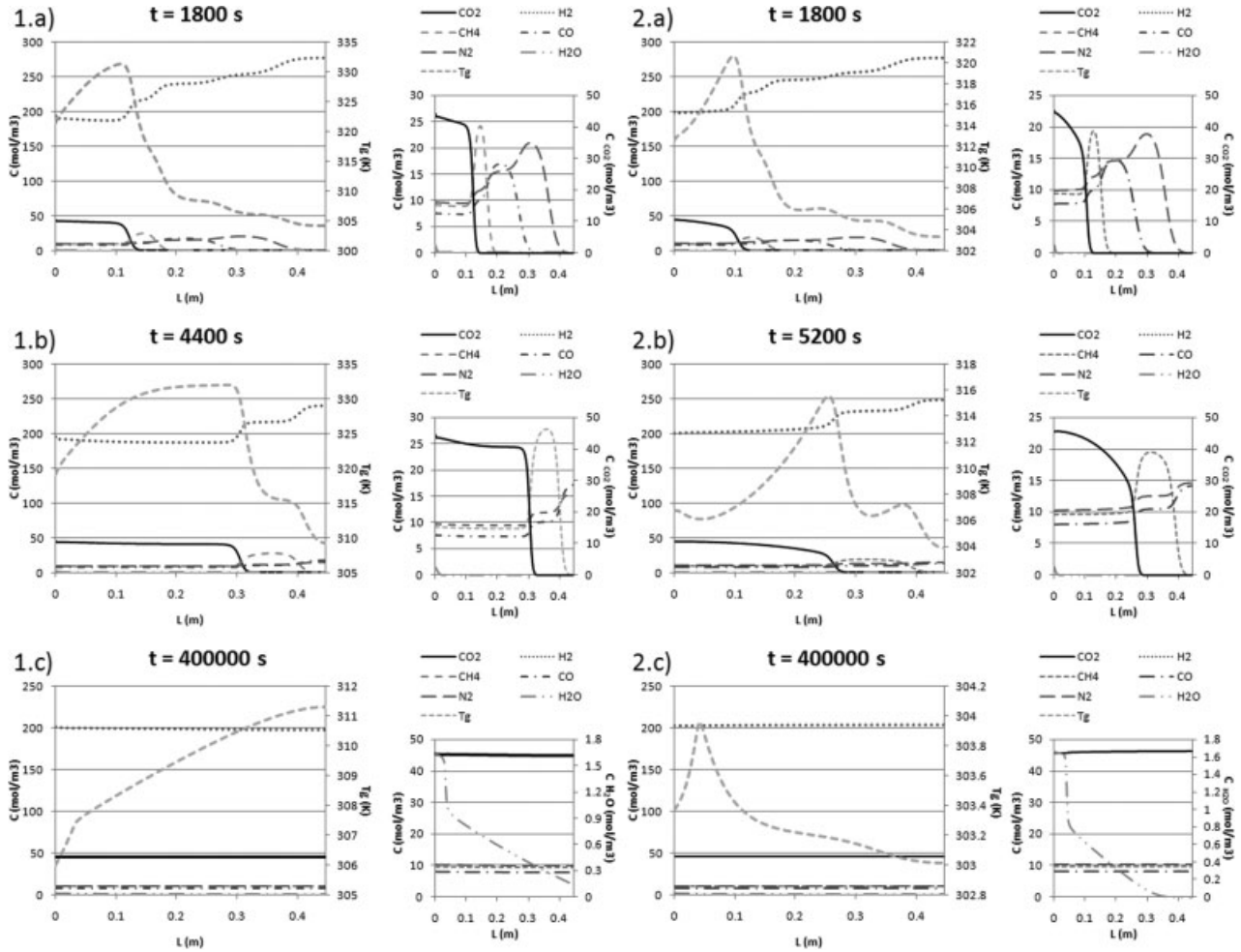

Figure 2. Concentration and temperature profiles obtained along the bed at different times for the adiabatic (1) and nonadiabatic (2) simulation with $\tau = 160$ s and the feed saturated with water.

throughout the bed. The molar specific heat of the adsorbed gas was assumed to be equal to the molar specific heat in the gas phase.[26]

The mathematical model was implemented in gPROMS environment (Process System Enterprise, London, UK) and numerically solved using the orthogonal collocation on finite elements method. The number of elements used was 90 with third order polynomials (two interior collocation points).

Figure 1 shows the molar flow rate and temperature histories at the column outlet obtained from the simulations with $\tau = 160$ s. Both adiabatic and nonadiabatic conditions were considered. For comparison purposes simulations with dry feed instead of saturated with water were also performed. The concentration and temperature profiles obtained along the bed at different times are shown in Figure 2 (1) and (2) respectively for adiabatic and non adiabatic conditions for the simulations performed with the feed saturated with water. In all these simulations the column was assumed to be initially filled with helium.

From these graphics it can be seen that the presence of the water vapor does not affect significantly the breakthrough behavior of the other species. Even when the carbon dioxide breaks through the bed, the water vapor front is still close to the inlet of the bed. This is due to the low amount of water fed to the column (at 303 K the saturation pressure is 0.0416 bar which corresponds to a feed molar fraction of only 0.6%) and also to the high adsorption capacity of the activated carbon towards water vapor. Thus a much higher stoichiometric time results for water which is in the case considered equal to ~772.5 h. However, the breakthrough time of water, although still much longer than the breakthrough time of the other compounds, occurs much earlier than the stoichiometric time (63 and 125 h, respectively for adiabatic and nonadiabatic conditions). This is due to the shape of the adsorption isotherm, unfavorable at low partial pressures and then favorable at the higher humidity region (Type V), which is reflected on the breakthrough curves. That is, the breakthrough curve is composed of two parts, the first part is dispersive and the second is a compressive front or shock.

Comparing the adiabatic and nonadiabatic simulations, a temperature increase of 35 K is observed in the first case, while in the second case the largest temperature increase due to the adsorption of carbon dioxide is only of 15 K. The much larger temperature increase observed for the adiabatic operation, causes the different impurities to break through

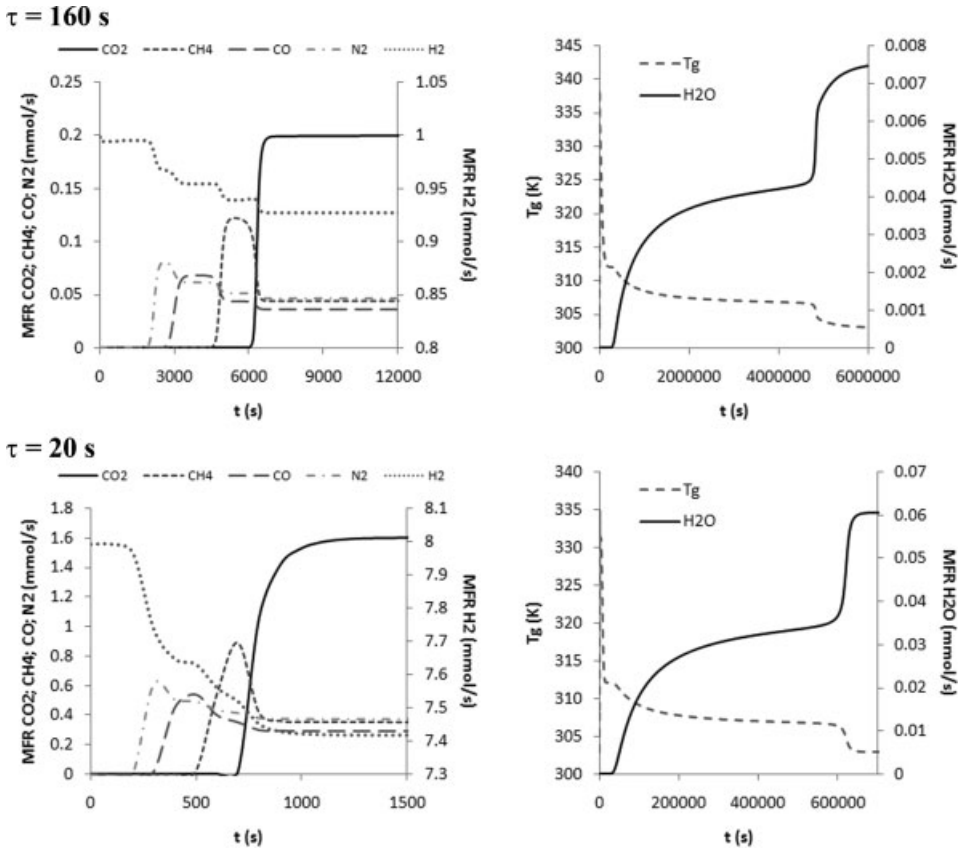

Figure 3. Molar flow rate and temperature histories at the column outlet obtained from the simulations with the different feed flow rates. The feed stream was saturated with water and adiabatic operation was considered.

the bed at shorter times. Also the resulting fronts in the case of adiabatic operation are sharper than for nonadiabatic conditions. However, these differences are almost negligible for the limiting contaminant (nitrogen).

The low temperature increase due to the adsorption of water vapor should also be pointed out. It can be seen that the compressive front of the water is accompanied by a temperature increase of 1 K in the case of the nonadiabatic operation and by a temperature front of 4 K in the case of adiabatic operation.

The simulations performed at different flow rates are compared in Figure 3, where the molar flow rate and temperature histories at the column outlet are shown. In these simulations, the feed was assumed saturated with water, adiabatic operation was considered and also the bed was presumed initially filled with hydrogen with the adsorbent in equilibrium. These graphics show the shortening of the breakthrough time as the feed flow rate increases and also the increase in dispersive behavior.

PSA simulations

The simulation of a PSA process will be now considered. An eight steps cycle, as schematically represented in Figure 4 (top), was used. The duration of each step was set taking

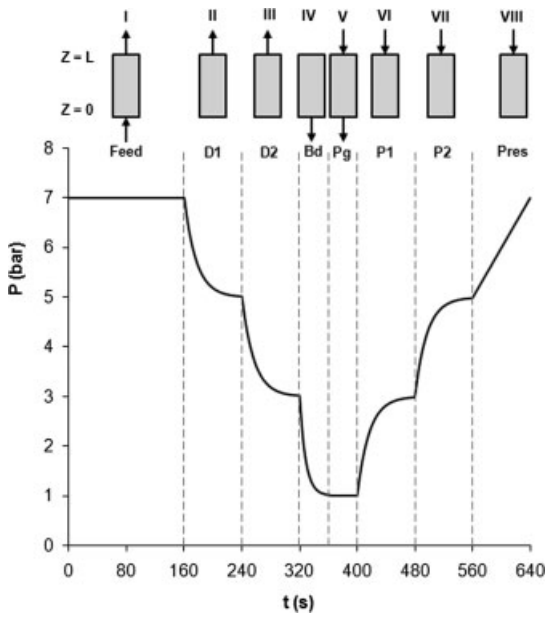

Figure 4. Cycle sequence used in the PSA simulations (top); pressure evolution along the PSA cycle at the column outlet for run 1 (bottom).

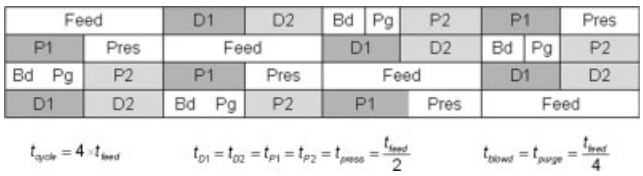

Figure 5. Four columns arrangement with continuous feed using the cycle sequence presented in Figure 4.

into consideration the extension of the cycle to a four columns process. This extension is shown in Figure 5. The operating conditions as well as the transport parameters were the same as the ones employed in the breakthrough simulations (given respectively in Table 3 and Table 4). High and low pressure values of 7 and 1 bar respectively were used. The bed was assumed initially filled with hydrogen with the adsorbent in equilibrium. Simulations at different feed flow rates, for which the feed duration was adjusted, and either under adiabatic or nonadiabatic conditions were performed. Dry feed was also considered in one simulation. The simulations performed are summarized in Table 5. The computational time required for each simulation is very long. Thus, as a first assessment of the system behavior, simulations considering only one column, for which the inlet streams of the purge and pressurization steps were assumed to be pure hydrogen, were performed. Although these simulations do not take into account the impurities present in the recycled streams of the continuous four columns process, when searching for the appropriate operating conditions to achieve the required product purity, the results obtained from the single column simulations are not far from reality in the case of hydrogen purification. Of course the presence of even a small amount of impurities has some effect on the process performance which must be evaluated. For this reason some results of simulations considering four columns with the corresponding recycling stream are also reported.

The process performance was evaluated by the hydrogen purity and recovery and by the adsorbent productivity,[27] defined respectively by Eqs. 14–16 and the results obtained are also shown in Table 5.

$$\text{PURITY} = \frac{\int_0^{t_{feed}} C_{H_2} u_0|_{z=L} dt}{\sum_{i=1}^{n} \int_0^{t_{feed}} C_i u_0|_{z=L} dt} \tag{14}$$

RECOVERY

$$= \frac{\int_0^{t_{feed}} C_{H_2} u_0|_{z=L} dt - \int_0^{t_{feed}} C_{H_2} u_0|_{z=L} dt - \int_0^{t_{purge}} C_{H_2} u_0|_{z=L} dt}{\int_0^{t_{feed}} C_{H_2} u_0|_{z=0} dt} \tag{15}$$

PRODUCTIVITY

$$= \frac{\left(\int_0^{t_{feed}} C_{H_2} u_0|_{z=L} dt - \int_0^{t_{press}} C_{H_2} u_0|_{z=L} dt - \int_0^{t_{purge}} C_{H_2} u_0|_{z=L} dt \right) A_{bed}}{t_{total} w_{ads}} \tag{16}$$

The pressure evolution along one cycle at the column outlet for run 1 is shown in Figure 4 (bottom) and the evolution of the hydrogen purity and recovery values with the simulation cycle number in Figure 6. It can be seen that even after 1052 cycles the cyclic steady state was not reached. Because of the long simulation times and also to the fact that the values of the performance parameters do not change significantly after around cycle number 300 (and thus an evaluation of the process performance can be assessed) the other simulations were stopped earlier.

The single column results show that the hydrogen purity required (99.99+%) is achieved in simulations 1–5. However, in the case of the simulation with the highest feed flow rate (15.08 SLPM) this high purity is only obtained if a smaller amount of feed is handled per cycle. If the feed time is increased (run 6) to match the amount of feed handled in runs 1–3, a reduction in the product purity is observed. Comparing the simulations performed with a feed flow rate of 7.54 SLPM, it can be seen that no significant difference is encountered in the performance parameters values obtained, that is, the use of either adiabatic or nonadiabatic conditions and the inclusion of water in the feed streams does not affect much the process performance. In all cases a process recovery of around 71% and an adsorbent productivity of $\sim$64 $mol_{H_2}/kg_{ads}/day$ are obtained. However, as mentioned earlier and also as will be seen below, when water is present the process did not yet reach cyclic steady state and water is still accumulating in the bed from cycle to cycle. From Table 5 it can also be seen that the decrease on feed flow rate to 1.88 SLPM results in a significant loss of productivity without any notable gain in recovery (bellow 2%). On the other hand, if the feed flow rate is increased to 15.08 SLPM,

Table 5. Conditions Used in the PSA Simulations and Hydrogen Purity and Recovery and Adsorbent Productivity Obtained

Run	P_{high} (bar)	P_{low} (bar)	Q_{feed} SLPM	Q_{purge} SLPM	t_{feed} (s)	Conditions	Cycles ran	Pur H_2 (%)	Rec H_2 (%)	Prod (mol/kg/day)
1*	7	1	7.54	2.15	160	adiab.	1052	99.9979	71.3	63.9
2*	7	1	7.54	2.15	160	nonadiab.	773	99.9985	71.0	63.5
3*	7	1	7.54	2.15	160	dry/adiab.	546	99.9980	71.7	64.4
4*	7	1	15.08	4.30	60	adiab.	311	99.9985	64.3	113
5*	7	1	1.88	0.54	700	adiab.	386	99.9989	72.7	16.4
6*	7	1	15.08	4.30	80	adiab	418	99.9631	73.0	130
7†	7	1	7.54	2.15	160	adiab.	530	99.8193	71.8	64.4
8†	7	1	7.54	2.15	140	adiab.	282	99.9737	68.1	60.6
9†	7	1	7.54	2.15	120	adiab.	251	99.9992	62.7	55.2

*1 column simulation.
†4 columns simulation.

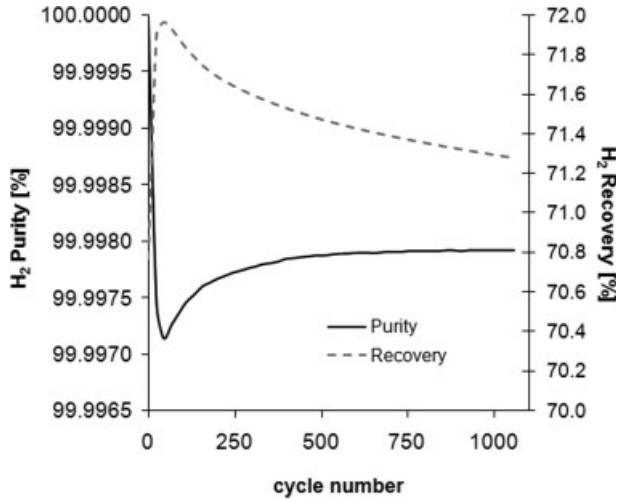

Figure 6. Evolution of the hydrogen purity and recovery values with the simulation cycle number for run 1.

there is an important increase in productivity, but the recovery also significantly decreases to 64%.

The four columns simulations show a reduction on the hydrogen purity obtained from 99.9979% to 99.8193% due to "dirty" streams recycling (run 1 versus run 7). To achieve the required purity, the feed duration needs to be reduced to 120 s. With this operating schedule, product purity and recovery, and adsorbent productivity respectively of 99.9992 %, 62.7%, and 55.2 mol_{H_2}/kg_{ads}/day are obtained.

The results obtained for the simulation "run 1" will now be detailed in Figures 7–9. Namely Figure 7 and Figure 8 show respectively the gas phase concentration/adsorbed phase concentration (for the major compounds CO_2 and H_2, the limiting contaminant N_2 and H_2O) and gas phase/wall temperature profiles obtained along the bed at the end of each step for cycle 1052. In Figure 9 the evolution of the adsorbed phase concentration (for hydrogen, carbon dioxide, nitrogen, and water vapor) and gas phase temperature profiles at the end of the feed step with the cycle number can be seen.

From all these graphics, several aspects can be pointed out. The regeneration of the bed from the feed to the purge step can be seen as well as the increase/decrease of temperature caused by the adsorption/desorption of the several impurities. Temperature oscillations of over 25 K are observed in the bed. This temperature profile affects the water concentration profiles, both in the gas phase and in the adsorbed phase (the adsorption equilibrium is strongly affected by the temperature). Another result that can be seen is that the amount of water adsorbed does not visually change from step to step, although the gas phase concentration profiles do change. This is due to the fact that the decrease in gas concentration is also accompanied by a decrease in temperature that affects the relative humidity. Actually the concentration profiles change but the relative humidity profiles do not change significantly (see Figure 10). The direct relation of the water adsorption equilibrium amount to the value of the relative humidity accompanied by the fact that large amounts of water are accumulated in the solid justifies the unusual result obtained.

From the evolution of the different profiles, it can be observed that the water accumulates slowly in the solid as the cycles proceed. This increase in the amount of water adsorbed affects the adsorption equilibrium of the other compounds, which is higher at the bed inlet in the initial cycles.

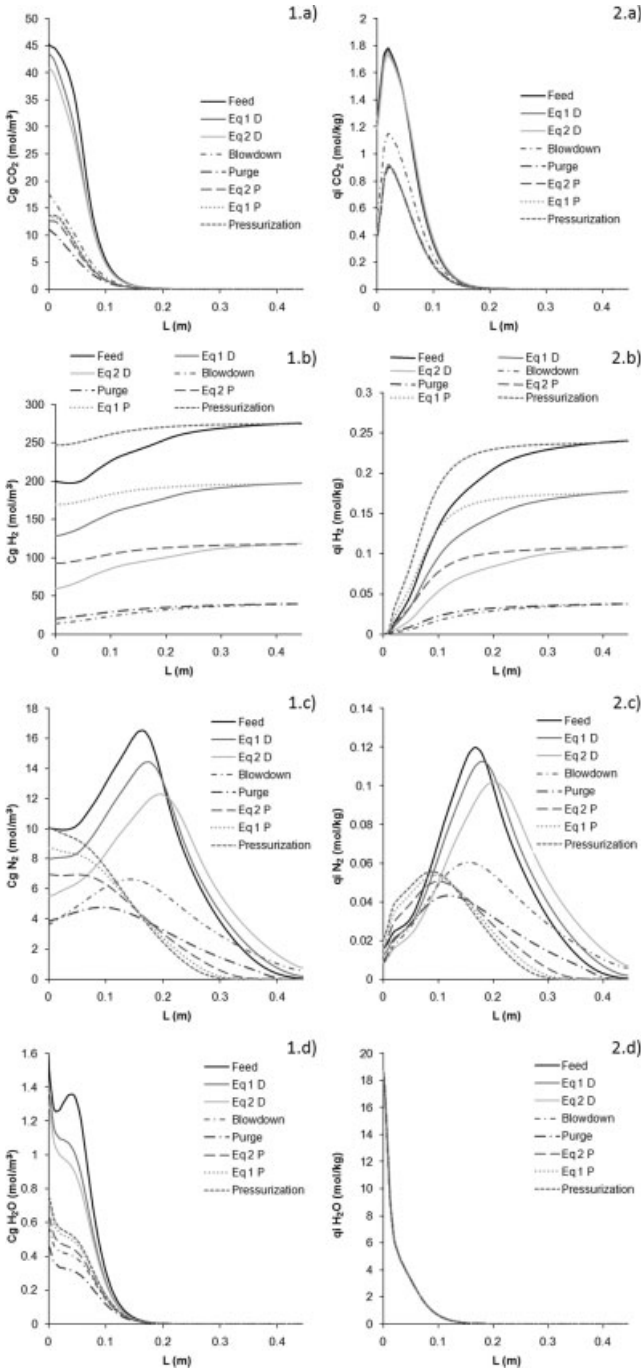

Figure 7. Gas phase concentration profiles (1) and adsorbed phase concentration profiles (2) obtained along the bed at the end of each step for cycle 1052 of run 1: (a) CO_2, (b) H_2, (c) N_2, and (d) H_2O.

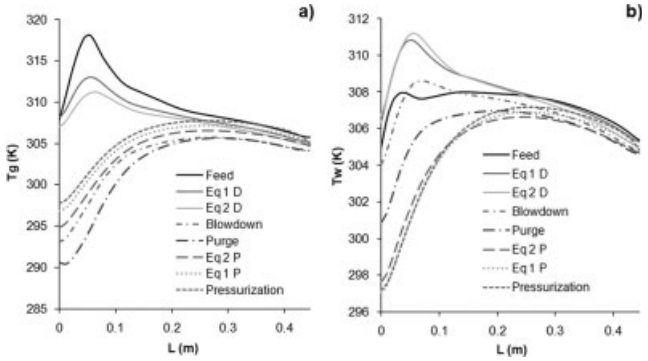

Figure 8. Temperature profiles obtained along the bed at the end of each step for cycle 1052: (a) gas phase and (b) wall.

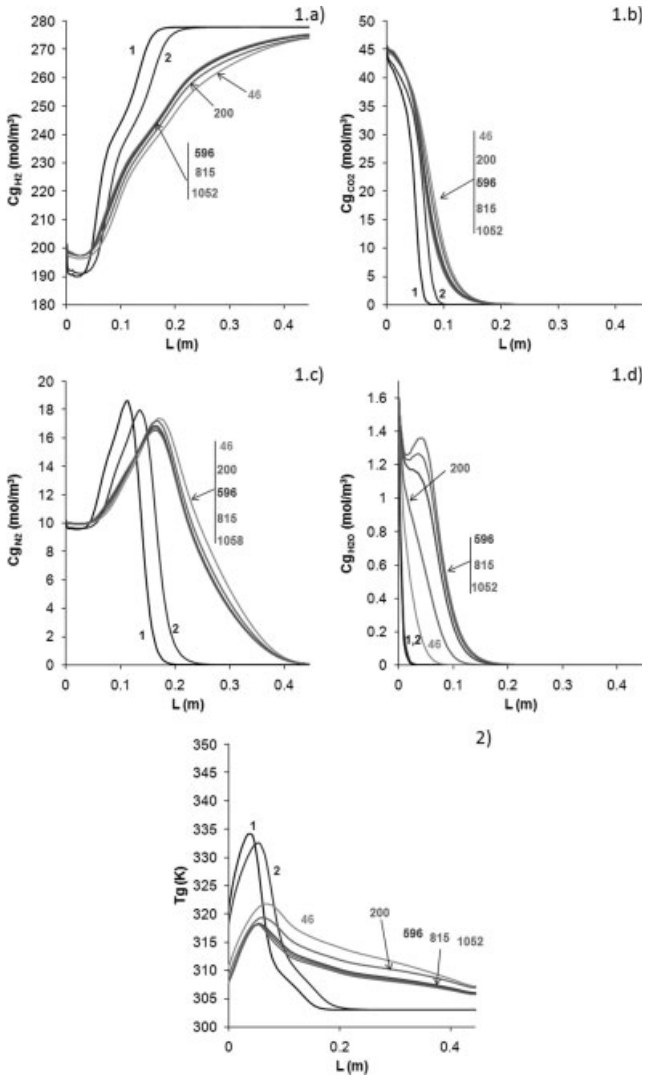

Figure 9. Evolution of the adsorbed phase concentration profiles (1) and evolution of the gas temperature profiles (2) at the end of the feed step with the cycle number for run 1: (a) hydrogen (b) carbon dioxide; (c) nitrogen and (d) water.

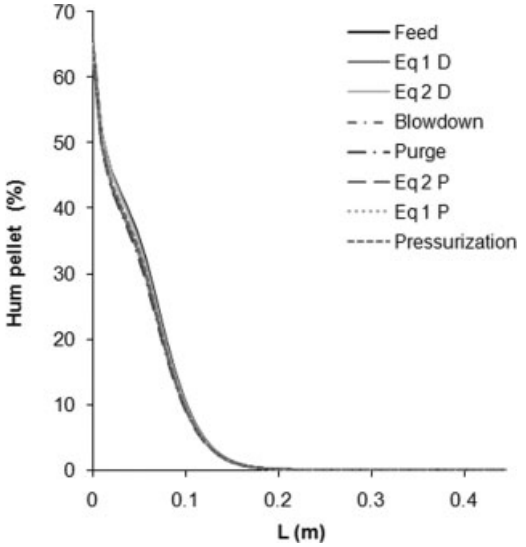

Figure 10. Relative humidity profiles inside the pellet obtained along the bed at the end of each step for cycle 1052 for run 1.

The fact that cyclic steady state has not been reached after 1052 cycles can also be seen from the progression of the water vapor fronts. The temperature profiles have however already stabilized. The temperature profiles are higher in the initial cycles, pushing the impurities fronts forward in the bed. As the bed temperature decreases, the adsorbent equilibrium capacity improves which allows for the impurity fronts to move slightly back. This effect is directly connected to the initial decrease in product purity followed by a slight improve of process performance observed in Figure 6.

The results showed that the presence of water vapor does not affect significantly the performance of the process due to the small amount of water in the feed. However, this conclusion is valid only during a limited time. As the cycles proceeded, water is accumulating in the bed and its presence affects severely the adsorbent capacity to adsorb and separate the other impurities. Thus from time to time, a more efficient regeneration procedure (for example, heating of the bed) must be performed to remove the accumulated water and avoid a decrease in the process performance.

Conclusions

A mixture of $H_2/CO_2/CH_4/CO/N_2$ saturated in water vapor was studied to supply knowledge of the fundamental adsorption behavior of these gases for hydrogen purification. Simulations results of fixed bed behavior and of an eight steps (including two pressure equalizations) PSA process were presented. The adsorbent considered was an activated carbon specially prepared to enhance the adsorption capacity of the impurities involved in the tackled process.

The fixed bed simulation results showed that the presence of water vapor did not affect significantly the breakthrough behavior of the other species due to the low amount of water in the feed stream and also to the high adsorption capacity of the activated carbon towards water vapor. It was also observed that adiabatic operation causes the different impurities to

break through the bed at shorter times when comparing to the nonadiabatic situation due to the larger temperature excursions observed in the first case. This difference is, however, almost negligible for the limiting contaminant (nitrogen).

In the single column PSA simulation with a feed flow rate of 7.54 SLPM and considering adiabatic operation, a 99.9979% purity hydrogen stream was attained at the end of the feed step for a process hydrogen recovery of 71.3% and an adsorbent productivity of 63.9 mol_{H_2}/kg_{ads}/day. It was observed that these process performance parameters are almost unaffected by the use of nonadiabatic operation or dry feed. However, it could also be seen that even after more than 1000 cycles, the process did not reach cyclic steady state. Water vapor was still accumulating in the bed. Thus more efficient regenerations should be performed periodically to avoid a decrease in process performance.

The single column simulations do not take into account the small amount of impurities in the recycling streams. When this effect is taken into consideration with the four columns simulations, a reduction on the hydrogen purity from 99.9979% to 99.8193% is observed. With the operating conditions considered the feed duration should be reduced in order to attain the required hydrogen purity. If a feed time of 120 s is employed, a product purity, recovery and productivity, respectively of 99.9992%, 62.7%, and 55.2 mol_{H_2}/kg_{ads}/day were obtained.

Acknowledgments

The authors like to acknowledge the financial support from European Commission through the FP6 funded project HY2SEPS (SES6-019887).

Literature Cited

1. Sircar S, Waldron WE, Rao MB, Anand M. Hydrogen production by hybrid SMR-PSA-SSF membrane system. *Sep Purif Technol*. 1999;17:11–20.
2. Ruthven DM, Farooq S, Knabel KS. *Pressure Swing Adsorption*. New York: VCH Publishers, 1994.
3. Yang RT. Gas separation by adsorption processes. Boston: Butterworths, 1987.
4. Yang J, Han S, Cho C, Lee C-H, Lee H. Bulk separation of hydrogen mixtures by one-column PSA process. *Sep Technol*. 1995;5:239–249.
5. Warmuzinski K, Tanczyk M. Multicomponent pressure swing adsorption. Part I. Modelling of large-scalle PSA instalations. *Chem Eng Process*. 1997;36:89–99.
6. Yang J, Lee C-H. Adsorption dynamics of layered bed PSA for H_2 recovery from coke oven gas. *AIChE J*. 1998;44:1325–1334.
7. Park J-H, Kim J-D, Yang RT. Adsorber dynamics and optimal design of layered beds for multicomponent gas adsorption. *Chem Eng Sci*. 1998;53:3951–3963.
8. Malek A, Farooq S. Hydrogen purification from refinery fuel gas by pressure swing adsorption. *AIChE J*. 1998;44:1985–1992.
9. Ahn H, Lee C-H, Seo B, Yang J, Baek K. Backfill cycle of layered bed H_2 PSA Process. *Adsorption*. 1999;5:419–433.
10. Park J-H, Kim J-N, Cho S-H. Performance analysis of a four-bed H_2 PSA process using layerd beds. *AIChE J*. 2000;46:790–802.
11. Lee J-J, Kim M-K, Lee D-G, Ahn H, Kim M-J, Lee C-H. Heat-exchange pressure swing adsorption process for hydrogen separation. *AIChE J*. 2008;54:2054–2064.
12. Stepanek F, Kubicek M, Marek M, Soos M, Rajniak P, Yang RT. On the modeling of PSA cycles with hysteresis-dependent isotherms. *Chem Eng Sci*. 2000;55:431–440.
13. Rege SU, Yang RT, Qian K, Buzanowski MA. Air-prepurifiaction by pressuer swing adsorption using sigle/layered beds. *Chem Eng Sci*. 2001;56:2745–2759.
14. Wilson SJ, Beh CCK, Webley P, Todd RS. The effect of a readily adsorbed trace component (water) in a bulk separation PSA process: The case of oxygen VSA. *Ind Eng Chem Res*. 2001;40:2702–2713.
15. Li G, Xiao P, Webley P, Zhang J, Singh R, Marshall M. Capture of CO2 from high humid flue gas by vacuum swing adsorption with zeolite 13X. *Adsorption*. 2008;14:415–422.
16. European ResearchProject HY2SEPS (Hybrid Hydrogen Carbon Dioxide Separation Processes). Available at: http://hy2seps.iceht.forth.gr/.
17. Lopes FVS, Grande CA, Ribeiro AM, Oliveira ELG, Loureiro JM, Rodrigues AE. Enhancing capacity of activated carbons for hydrogen production. *Ind Eng Chem Res*. 2009; 48:3978–3990.
18. Kiselev FP. Vapor adsorption on zeolites considered as crystalline species adsorbents Molecular Sieve Zeolites-II. *ACS Symp Ser*. 1971;102:37–68.
19. Barrer RM. Sorption in porous crystals: equilibria and their interpretation. *J Chem Technol Biotechnol*. 1981;31:71–85.
20. Taqvi SM, LeVan MD. Virial description of two-component adsorption on homogeneous and heterogeneous surfaces. *Ind Eng Chem Res*. 1997;36:2197–2206.
21. Da Silva FA. *Cyclic Adsorption Processes: Application to Propane/Propylene Separation*. Portugal: University of Porto, 1999.
22. Wakao N, Funazkri T. Effect of fluid dispersion coefficients on particle-to-fluid mass transfer coeficients in packed beds. *Chem Eng Sci*. 1978;33:1375–1384.
23. Wasch APD, Froment GF. Heat transfer in packed beds. *Chem Eng Sci*. 1972;27:567–576.
24. Bird RB, Stewart WE, Lightfoot EN. *Transport Phenomena*, 2nd ed. Singapore: Wiley, 2002.
25. Ruthven DM. *Principles of Adsorption and Adsorption Processes*. New York: John Wiley & Sons, 1984.
26. Sircar S. Excess properties and thermodynamics of multicomponent gas adsorption. *J Chem Soc Faraday Trans*. 1985;81:1527–1540.
27. Rota R, Wankat PC. Intensification of pressure swing adsorption processes. *AIChE J*. 1990;36:1299–1312.

Manuscript received Oct. 17, 2008, and revision received Feb. 12, 2009.